

# A comparative study of the adhesion of biosynthesized gold and conjugated gold/prodigiosin nanoparticles to triple negative breast cancer cells

S. O. Dozie-Nwachukwu<sup>1,2</sup> · J. D. Obayemi<sup>1,3</sup> · Y. Danyuo<sup>1,4</sup> · N. Anuku<sup>5</sup> · O. S. Odusanya<sup>1,2</sup> · K. Malatesta<sup>5</sup> · W. O. Soboyejo<sup>1,3,5</sup>

Received: 19 May 2017 / Accepted: 27 June 2017 / Published online: 17 August 2017  
© Springer Science+Business Media, LLC 2017

**Abstract** This paper explores the adhesion of biosynthesized gold nanoparticles (AuNPs) and gold (Au) nanoparticle/prodigiosin (PG) drug nanoparticles to breast cancer cells (MDA-MB-231 cells). The AuNPs were synthesized in a record time (less than 30 s) from *Nauclea latifolia* leaf extracts, while the PG was produced via bacterial synthesis with *Serratia marcescens* sp. The size distributions and shapes of the resulting AuNPs were characterized using transmission electron microscopy (TEM), while the resulting hydrodynamic diameters and polydispersity indices were studied using dynamic light scattering (DLS). Atomic Force Microscopy (AFM) was used to study the adhesion between the synthesized gold nanoparticles (AuNPs)/LHRH-conjugated AuNPs and triple negative breast cancer cells (MDA-MB-231 cells), as well as the adhesion between LHRH-conjugated AuNP/PG drug and MDA-MB-231 breast cancer cells. The adhesion forces between LHRH-conjugated AuNPs and breast cancer cells are shown to be

five times greater than those between AuNPs and normal breast cells. The increase in adhesion is shown to be due to the over-expression of LHRH receptors on the surfaces of MDA-MB-231 breast cancer cells, which was revealed by confocal immuno-fluorescence microscopy. The implications of the results are then discussed for the selective and specific targeting and treatment of triple negative breast cancer.

## 1 Introduction

Significant efforts have been made to develop gold nanoparticles (AuNPs) and conjugated AuNPs/cancer drug nanoparticles for the specific and selective targeting of cancer [1–3]. In most cases, gold has been used due to its photo-optical properties and biocompatibility [4]. AuNPs have also been synthesized by chemical, physical and biological pathways [5–8].

Although most of the prior efforts to synthesize AuNPs have used chemical synthesis [9] and physical synthesis [10], there is growing interest in the biosynthesis of AuNPs from plants [11–13], microbes [14] and fungi [15]. These approaches have been used to produce AuNPs with different sizes and shapes [16, 17]. Gold nanoparticles have also been shown to interact with laser beams to induce heat for hyperthermic cancer treatment [18], laser surgery [19] and drug delivery [20].

In most cases, fungi [21], actinomycetes [22], and bacteria [23] have been used to synthesize metallic nanoparticles [24]. Some prior work [13, 22, 25, 26] has also explored the use of parts of plants, or whole plants, in the synthesis of AuNPs. Such plant-based synthesis, using plant extracts, is relatively under-exploited. It could also be

✉ W. O. Soboyejo  
soboyejo@princeton.edu

<sup>1</sup> Department of Materials Science and Engineering, African University of Science and Technology (AUST) Abuja-Nigeria, Abuja, Nigeria  
<sup>2</sup> Biotechnology Advanced Research Center, Sheda Science and Technology Complex (SHESTCO) P.M.B 186, Garki, Abuja, Nigeria  
<sup>3</sup> Department of Mechanical and Aerospace Engineering, Olden Street, Princeton, NJ 08544, USA  
<sup>4</sup> Department of Materials Science and Engineering, Kwara State University, Malete, Nigeria  
<sup>5</sup> Princeton Institute of Science and Technology of Materials (PRISM), Bowen Hall, 70 Prospect Street, Princeton, NJ 08544, USA

adapted in low-resource settings and developing countries for the synthesis of metallic nanoparticles.

Furthermore, the plant-based synthesis of AuNPs has been shown to be easier than the microbial-based synthesis of AuNPs. This is because the process occurs relatively quickly, and does not involve the use of bioreactors, as in the case of microbial synthesis [27]. The use of plant extract method also is a technique that is relatively easy to scale up [20, 28].

A number of plants have been used to synthesize AuNPs [29–35]. They include: leaf extracts of Tamarind (*Tamarindus indica*) [31], *Cinnamomum camphora* [32], lemongrass (*Cymbopogon flexuosus*) [28], geranium (*Pelargonium graveolens*) [32], extract of *Emblia officinalis* [33], Neem (*Azadirachta indica*) [34] and *Aloe vera* [35]. All of these plant extracts have been shown to have the potential to reduce Au<sup>3+</sup> ions to AuNPs.

In our recent work [27], AuNPs were synthesized from *Nauclea latifolia* leaf extracts. The effects of pH on the sizes and shapes of the AuNPs were also explored. The AuNPs that were synthesized at pH values between 4.5 and 9.5 resulted in nanoparticles with sizes between 10 and 60 nm. Furthermore, extracts from the NL leaf were also shown to have anticancer activity and/or therapeutic activity [36–38]. These two-in-one effects suggest that the bio-synthesis of AuNPs can be combined with the drugs to produce nanoclusters that are conjugated to attach specifically to receptors on cancer cells [39] or diseased cells [40]. There is, therefore, a potential to develop such AuNPs for the specific targeting and treatment of cancer.

Although, AuNPs are being considered for potential applications in laser hyperthermia, significant efforts have also been made to develop Au/cancer drug nanoparticles that can be used for both laser hyperthermia and cancer drug release [41, 42]. There is, therefore an interest in the synthesis of Au/cancer drug nanoparticles that can be used for both cancer drug release and laser hyperthermia. Hence, in this paper we explore the synthesis of AuNPs/prodigiosin cancer drug for the specific targeting and treatment of triple negative breast cancer cells via localized drug delivery and laser hyperthermia.

Furthermore, in an effort to understand the specific targeting of the breast cancer cells, the adhesion of the nanoparticles was studied along with the shapes and sizes of AuNPs/PG drug prepared under different pH conditions. The latter were characterized using transmission electron microscopy images and dynamic light scattering. The adhesion of LHRH-conjugated gold nanoparticles is shown to be much greater than that of AuNPs to normal breast cancer cells. The increased adhesion of the LHRH-conjugated AuNPs and/or PG cancer drug is attributed to the increased incidence of LHRH receptors that are over-expressed on the surfaces of breast cancer cells. The

implications of the results are discussed for the specific/selective targeting and the localized treatment of triple negative breast cancer cells.

## 2 Theory

The adhesion measurement technique involves the use of atomic force microscope (AFM) to measure adhesion forces between nanoparticles coated on an AFM tip and breast cancer cells at a nanoscale. Force microscopy method involves bringing coated AFM tips close enough for adhesive interactions to occur [Fig. 1a and b]. Due to the presence of inherent Van der Waals forces present, the two components jump into contact [Fig. 1b].

After contact, the tips get displaced further, as they undergo elasticity in the same direction [43–45]. Upon their retraction, the displacements are reversed, as the loads are reduced to zero. However, because of the presence of adhesion, the tips do not detach at zero load. The tips only get retracted when the applied force applied is sufficient to overcome the adhesion. When this happens, the pull-off of the AFM tips occurs from the substrates.

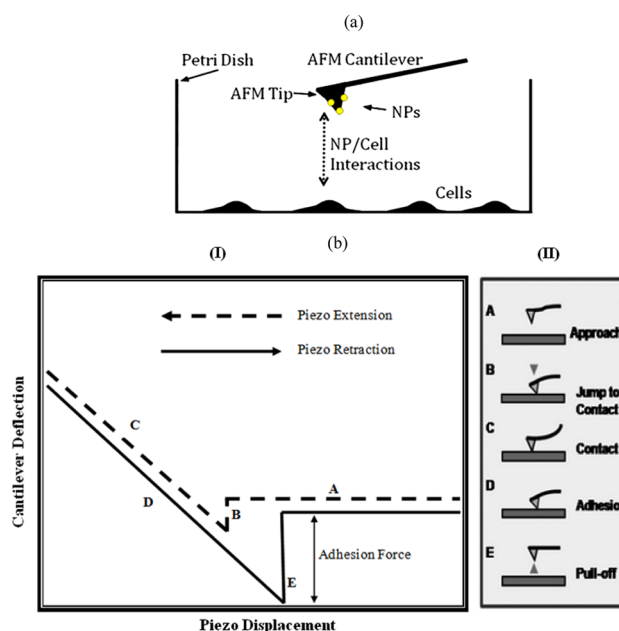


**Fig. 1** a Ligand/receptor interactions. In the experimental setup, ligands on the dip-coated AFM tip interact with surface receptors on breast cancer cells (MDA-MB-231)/normal breast cells (MCF10A) seeded on a Petri dish ([Adapted from Ref. [45]). b Schematic of typical force–displacement plot with corresponding stages of force displacement behavior. In one approach–retract cycle, the AFM tip approaches the surface of the sample (a), jumps to contact with the surface when significant van der Waals forces are felt (b), and undergoes elastic bending and is retracted (c, d). Due to adhesive interactions, the tip does not detach from the substrate until a force sufficient to pull the tip off of the surface is achieved (e). (Adapted from Ref. [43, 45])

The resulting pull-off force represented as  $F$ , is a measure of the adhesion between the nanoparticle/drug complex and the breast cancer/normal breast cells. This is given by Hooke's law to be:

$$F = k\delta \quad (1)$$

where  $k$  is the stiffness of the AFM cantilever and  $\delta$  is the displacement of the AFM tip at the onset of pull-off. The spring constants of the uncoated (bare) and coated AFM tips is usually determined experimentally using the thermal tune method [46]. Thermal tuning is done to obtain the actual spring constants ( $k$ ) that are subsequently used to calculate the pull-off forces (adhesion forces) from the Hooke's equation above. The  $k$  value is usually obtained at a temperature of 22 °C and a steady relative humidity of 36–45%. Usually, prior to each adhesion measurement, the photo-detector sensitivity was calibrated using a stiff quartz material.

It is important to note that measurements of pull-off (adhesion forces) have been used to measure forces in biological materials [47–49]. These have been shown to be sufficient to detect the differences between breast cancer cells and normal breast cells in recent work by Meng et al. 2010 [44]. They have also been shown to reveal differences between the adhesive and cohesive interactions in different nanoclusters of gold nanoparticles in recent work by Oni et al. 2014 [45].

However, although atomic force microscopy has been used to measure the adhesive forces between the constituents of nanoclusters, to the best of our knowledge, there have been no prior measurements of the adhesion forces between LHRH-conjugated gold nanoparticles and triple negative breast cancer cells/normal breast cells. These will, therefore, be measured in the current work, with the objective of determining the robustness of gold nanoparticle clusters for the specific targeting and treatment of cancer via localized chemotherapy and hyperthermia.

### 3 Experimental procedures

#### 3.1 Materials

The gold (III) chloride trihydrate, ACS reagent,  $\geq 49.0\%$  Au basis, was purchased from Sigma-Aldrich, St. Louis, USA, Lot number 127K1374. The other materials include: distilled water and mature leaves of *Nauclea latifolia* (obtained from SHESTCO, Abuja, Nigeria). Phosphate buffer and Acetate buffer for synthesis were obtained from Sigma-Aldrich (St. Louis, MO, USA), and Thermo Fisher Scientific, Inc. (Waltham, MA, USA), respectively. Cyclohexane Mercaptan, 99% for conjugation work was purchased from

Acros Organics, Thermo Fisher Scientific (New Jersey, USA).

The LHRH peptides that were used for the conjugation and the immuno-fluorescence staining of LHRH receptors were purchased from Sigma-Aldrich Co. LLC, (St. Louis, MO, USA). In the case of the adhesion measurement, MDA MB 231 breast cancer cell line, MCF 10 A normal breast cell line, growth media (L15), and medium supplements (fetal bovine serum and penicillin/streptomycin) were all purchased from American Type Culture Collection (ATCC, Manassas, VA, USA). Also, uncoated antimony (n)-doped Si atomic force microscopy (AFM) tips (MPP-31100) were purchased from Bruker AFM Probes (Santa Barbara, CA USA).

#### 3.2 Extraction and synthesis of gold nanoparticles

Details of the procedures that were used to obtain plant extracts from *Nauclea latifolia* are provided in Ref. 27. Hence, we will only summarize the procedures for the extraction and synthesis of the AuNPs from the *Nauclea latifolia* leaves. Although extracts for AuNPs synthesis can be obtained from both fresh leaves and dry ones, fresh mature leaves of *Nauclea latifolia* were used in this study. These were collected from the Botanical Park at Sheda Science and Technology Complex (SHESTCO), Gwagwada, Abuja, Federal Capital Territory, Nigeria. Some of the leaves were sun dried for 2 days, ground into powder with a pestle and mortar, before storing the ground powder in a bottle and refrigerated.

In the case of the fresh leaves, they were washed with sterile distilled water and ground with a mortar and pestle. 1 g of freshly ground leaves was placed in each of 7 beakers containing 20 ml of 0.5 M Acetate buffer (pH 4.0, 5.5, 6.5) and 0.5 M phosphate buffer solutions of pH ranges 7.5, 8.5 and 9.5, with the last flask containing distilled water, labelled as NLO (that is, without pH adjustment, though the pH was found to be 7.0). These were stirred at 500 rpm for 20 min on a magnetic stirrer. The leaf extracts were filtered through Whatmann filter paper No.1. The synthesis of AuNPs at pH 7.0 from *Nauclea latifolia* has been shown [27] to be promising for biomedical applications.

In the case of the dry leaves, 0.05 g (0.25%) of the dried *Nauclea latifolia* leaf powder was soaked in 20 ml of the corresponding buffer solutions (at different pH) and stirred on a magnetic stirrer for 20 min. The solutions were then filtered accordingly to obtain the extract.

Synthesis of AuNPs was achieved by using the extracts from the leaves prepared as described above. 4 ml of each of the fresh *Nauclea latifolia* extracts were measured into corresponding test tubes. Subsequently, 1 ml of 2.5 mM gold (III) chloride tri-hydrate was then added to each test tube at room temperature (28–30 °C). The *Nauclea latifolia*

leaf extract reacted with hydrogen tetra chloroaurate (HAuCl<sub>4</sub>) within 30 s forming AuNPs. This was revealed by the visible color change that occurred as HAuCl<sub>4</sub> solution changed color from pale yellow to ruby red.

### 3.3 Ligand conjugation of LHRH to gold nanoparticles

#### 3.3.1 Thiolation of gold nanoparticles

The thiolation and conjugation was done using AuNPs that were formed at a pH of 7.0. The conjugation process involved the use of a self-assembled monolayer (SAM) method developed originally by Shiao-wen et al. 2008 [50], with some modifications. Cyclohexane mercaptan, 99%, from Acros Organics was used. First, a 1 mM thiol solution was prepared by measuring 6 µl of the cyclohexane thiol in a fume cupboard, into 50 ml of 50% ethanol, and stirred at 500 rpm for 20 min to mix properly. In another 50 ml beaker, 10 ml of 5 mg/ml gold nanoparticles was added and placed on a magnetic stirrer that was set at 500 rpm. Then 2 ml of 1 mM thiol solution was then added and stirred for 30 min.

#### 3.3.2 Conjugation with LHRH

A 1 mg/ml solution of LHRH was freshly prepared in deionized water. Subsequently, 4 ml of the already thiolated gold nanoparticles was then poured into a beaker, before adding 1 ml of the LHRH solution. This was then stirred on the magnetic stirrer for 30 min at a temperature of 4 °C. This resulted in the coupling of LHRH to the gold core (using a thiol linkage), either through an amino acid added at the C-terminus, or a D-amino acid placed in position 6 of the LHRH peptide sequence.

### 3.4 Prodigiosin synthesis and prodigiosin/AuNP mixtures

#### 3.4.1 Prodigiosin (PG) synthesis

A method developed recently by Obayemi et al. 2016 [51] for the synthesis and purification of prodigiosin (PG) was adopted for the synthesis and purification of the PG used in this work. Hence, the synthesis and purification process will only be summarized in this paper. The extraction of PG was done from *Serratia marcescens* subsp. *marcescens* strain using the method described by Kamble et al. [52]. The extracted samples were then purified using size exclusion chromatography (using Sephadex G-50 superfine resin), prior to characterization with High Performance Liquid Chromatography (HPLC) using an HPLC system with a dual wavelength absorbance detector (Waters 2695 with 2487 Absorbance Detector, LabX, Midland, ON, Canada

The PG content was determined from the HPLC analysis by comparing the peak areas (normalization), as well as the symmetrical increase of the peak areas, as a function of the retention time.

#### 3.4.2 Mixture of prodigiosin and conjugated gold nanoparticles

Prodigiosin was added to the gold nanoparticles-conjugate by means of physisorption, whereby the molecules were held in place by Van der Waals forces. 1 mg of prodigiosin was dissolved in 2 ml of methanol and added to the gold nanoparticles conjugate. The mixture was stirred at 500 rpm at a temperature of 4 °C (to prevent the denaturation of proteins) for 30 min.

### 3.5 Gold nanoparticle characterization

#### 3.5.1 UV-spectrophotometry measurements

Following the synthesis and conjugation, an ultraviolet–visible spectrophotometer (UV–Vis) (CECIL 7500 Series, Buck Scientific Inc., East Norwalk, USA), with a range between 400 and 700 nm, was used to confirm the formation of gold nanoparticles. This was done using procedures described in detail in Ref. 27. The procedures were repeated at 20 min intervals for total durations of 1, 24 and 48 h.

#### 3.5.2 Transmission electron microscopy (TEM) and electron diffraction (ED)

The shapes and sizes of the nanoparticles were characterized using transmission electron microscopy (CM100 Transmission Electron Microscope, Philips/FEI Corporation, Hillsboro, OR, USA), while the presence of gold was confirmed again using selected-area electron diffraction (SAED) patterns of the nanoparticles. Prior to TEM examination, drops of gold nanoparticle solutions were placed on copper grids. These were allowed to dry under ambient conditions (25 °C). They were then mounted on a CM100 Transmission Electron Microscope at the Princeton Institute of Science and Technology of Materials (PRISM) at Princeton University, New Jersey, USA. Subsequently, the nanoparticle sizes and shapes were further analyzed using ImageJ software package (NIH Image, Scion Image for Windows, National Institute of Health, Bethesda, Maryland, USA). In the case of SAED analysis, a selected-area aperture, with a diameter of 1 mm, was used. The resulting SAED patterns were then recorded and analyzed.

### 3.5.3 Dynamic light scattering (DLS)

A Malvern Instrument Zeta-sizer Nano Series (Malvern Instruments, Westborough, MA, USA) was used in the DLS measurements of the AuNPs as well as conjugated AuNPs/PG mixtures at room temperature (25 °C). The samples were first diluted 1:8 with distilled water using a 1 mL pipette. They were then filtered with a 0.22 micron filter and in each case 0.1 mL of the gold nanoparticles solution was added into the cuvette. The wavelength at which the DLS instrument was run is 660 nm and the fixed scattering angle was used 90. 3 runs per sample were performed for 2:00 min per run, giving a total of 6:00 min per sample.

### 3.5.4 Energy dispersive X-ray spectroscopy (EDS)

An Environmental Scanning Microscope (ESEM) (Model FEI Quanta 200 F with Oxford-EDS system IE 250 X Max 80, Philips/FEI, Hillsboro, OR, USA) was used to obtain semi-quantitative estimates of the compositions of the AuNPs and LHRH-conjugated AuNPs/PG mixtures. Prior to EDS characterization, the AuNP solutions and the conjugated AuNP/PG mixtures were ultra-centrifuged at 12,000 rpm for 30 min. This was done to concentrate the nanoparticles. The nanoparticles were then placed on the SEM sample holder and air dried before viewing them in the ESEM.

## 3.6 Adhesion measurements

Prior to the adhesion measurements, a breast cancer cell line (MDA-MB-231 cells) and a normal-breast cell line (MCF 10 A cells) was cultured and prepared. About 20  $\mu$ l of  $5 \times 10^4$  cells/ml MDA-MB-231 cells was cultured in  $60 \times 15$  mm Falcon cell culture Petri dishes at 37 °C. This was done under standard atmospheric pressure in L-15 medium supplemented with 100 I.U./mL penicillin/100 g/mL streptomycin and 10% FBS.

In the case of the normal breast cells,  $5 \times 10^4$  cells/ml of MCF10A breast cells was incubated at 37 °C in 5% CO<sub>2</sub> in DMEM/F12 medium (Invitrogen # 11330-032) supplemented with 5% horse serum (Invitrogen # 16050-122), 30 ng/ml murine Epidermal Growth Factor (Peprotech #315-09), 0.5  $\mu$ g/ml hydrocortisone (Sigma, #H-0888), 100 ng/ml cholera toxin (Sigma #C8052-1MG), 10  $\mu$ g/ml insulin (Sigma #I-882-100MG), 1% Penicillin-Streptomycin (Invitrogen #15070-063), and 0.2% amphotericin (Gemini Bio-products, #400-104), respectively.

After 72 h of culturing, the cell confluence was about 70%. Both cell samples were then washed twice with PBS solution (1X PBS at 4 °C) and fixed in 3.7% formaldehyde solution for 15 min. The fixed cells were then rinsed three times with PBS (1X PBS at 4 °C). This was followed by

three rinses with distilled-deionized water (4 °C). This last rinse with water was used to remove possible salt deposits that may have resulted from the prior PBS rinses. Finally, the fixed cells were dried in a vacuum desiccator for 2 h (at 25–30 °C).

Adhesion measurements were done using a Multimode Dimension DI Nanoscope IIIa Atomic Force Microscope (Bruker Instruments, Woodbury, NY, USA). The Atomic Force Microscope (AFM) tips were coated with the LHRH, AuNPs, prodigiosin drug (PG), LHRH-conjugated AuNPs and LHRH-conjugated AuNPs/PG mixture using a simple dip coating technique [45]. This was done under sterile conditions at a temperature of 22 °C, as reported by Oni et al. [45].

To ensure that the AFM tips were coated with LHRH or LHRH-AuNPs, the bare AFM tips and the nanoparticle coated AFM tips were imaged using environmental scanning electron microscopy (ESEM). The secondary electron images of the coated and bare AFM tips were obtained from a Phillips FEI Quanta 200 Field Emission Gun (FEG) Environmental-SEM (Philips Electronics N.V., Eindhoven, Netherlands). These images were used to confirm the presence of LHRH and nanoparticle coatings on the AFM tips, before and after the adhesion measurements. The different coated tips were brought into contact with the substrates (breast cancer cells and normal breast cells) during the AFM adhesion measurements.

As described in Section 2, the Atomic Force Microscope (AFM) measures the deflection of a cantilever spring with a sharp AFM tip (the tip radius is about 10–100 nm) as a function of displacement from a horizontal position, which is driven by a piezo-electric system. The deflection of the cantilever is monitored using a laser-photodiode system. It relates the forces between the probe-tip and the substrate [53] to the displacement of the tip.

When the cantilever is far away from the surface of the sample, the AFM-tip is force free. Hence, there is no adhesive interaction between the tip and the substrate. However, as the tip approaches the surface, adhesion forces increase significantly. These attract the tip towards the substrate (See Fig. 1b). At a distance of a few nanometers from the substrate (~20 nm), the secondary forces (Van der Waals forces and hydrogen bonds) acting on the surface become significant, causing the cantilever and the tip to jump into contact with the sample surface [54].

The piezo drive pushes the AFM-tip further on the surface until a point of repulsion is reached and the motion of the piezo is reversed. The cantilever deflects towards the surface due to adhesion force before the tip breaks contact with the surface. The sudden pull-off may cause free vibrations of the cantilever. The pull-off is described as the adhesion between the coated AFM tips and surface of the substrate [52–57].

The following adhesion measurements were made:

- i. Bare AFM tip to breast cancer/normal breast cells;
- ii. LHRH-coated AFM tip to breast cancer/normal breast cells;
- iii. PG drug coated AFM tip to breast cancer/normal breast cells;
- iv. AuNPs to breast cancer/normal breast cells;
- v. AuNPs–LHRH to breast cancer/normal breast cells, and
- vi. AuNPs–LHRH/PG mixture to breast cancer/normal breast cells.

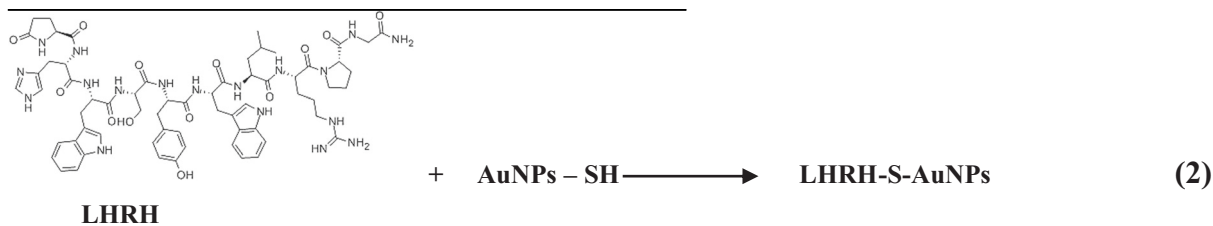
### 3.7 Confocal fluorescence microscopy of LHRH receptors

Immuno-fluorescence staining of both breast cancer cells and normal breast cells were carried out using methods reported earlier by Meng et al. 2010 [44]. Both triple negative breast cancer cells (MDA-MB-231 cells) and normal breast cancer cells (MCF 10 A cells) were cultured on sterile cover slips (with inside cross sectional areas of  $60 \times 15$  mm) and Falcon cell culture Petri dishes in their respective growth media described in section 3.6. After 48 h, the cells were fixed, stained and imaged, as reported by Meng et al. 2010 [44].

## 4 Results

### 4.1 Nanoparticle synthesis, conjugation and characterization

A period of 30 sec was used to synthesize the AuNPs from the *Nauclea latifolia* leaf extract [27]. This was possible when gold aurochloride ( $\text{HAuCl}_4$ ) reacted with the



extract at a pH of about 7.0. The formation of AuNPs was revealed by the visible color change that occurred, as the  $\text{HAuCl}_4$  solution changed from a pale yellow color to ruby red [27].

From the UV–Vis measurements, the peaks revealed that AuNPs were synthesized with a plasmon resonance peak at 540 nm. The nanoparticles remained stable at 540 nm after

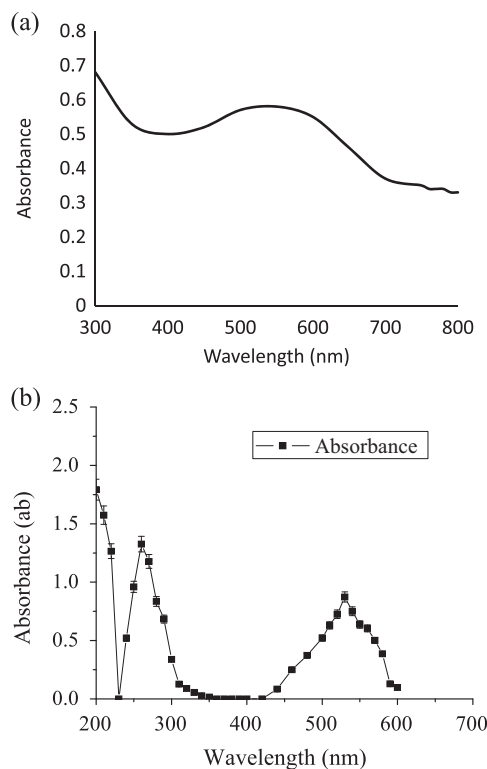
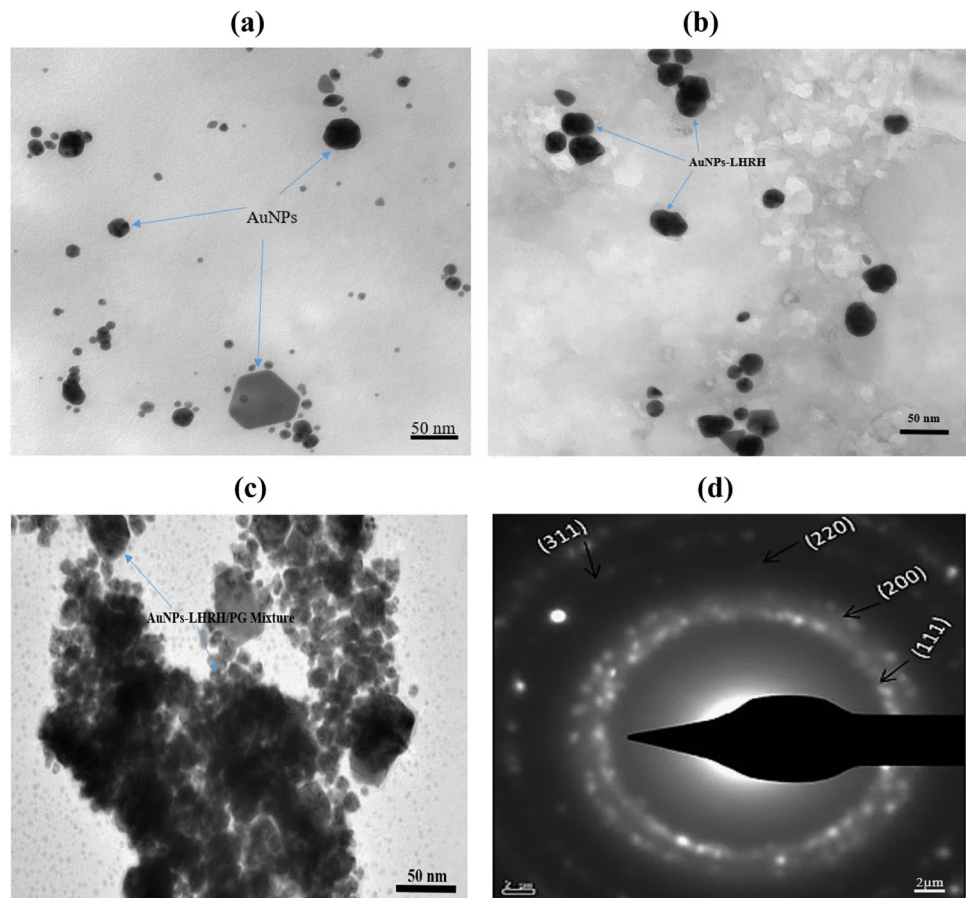


**Fig. 2** **a** UV/Vis spectra obtained for AuNPs produced from *Nauclea latifolia* leaves at a pH of 7.0; **b** UV/Vis spectra obtained for LHRH-conjugated AuNPs Synthesized in **a** above

48 h, though the absorbance increased with time. The UV results for both unconjugated AuNPs and LHRH conjugated AuNPs showed evidence of the presence of AuNPs (Fig. 2a). After conjugation, the UV–Vis spectra conjugation (Fig. 2b) showed the presence of 2 peaks, at 260 nm which confirms the presence of the peptide, LHRH [58], and a second peak at 544 nm which is the wavelength of AuNPs. The reaction schematics of conjugation of AuNPs to LHRH is represented below.

The TEM micrographs obtained for the AuNPs synthesized from *Nauclea latifolia* leaves, as well as the LHRH-conjugated AuNPs/PG mixtures, are presented in Fig. 3. After conjugation with LHRH, the average size of the conjugated AuNPs was within the range of 51–60 nm. The shapes of the AuNPs formed are combination of prismatic,

**Fig. 3** TEM images of **a** AuNPs synthesized from *Nauclea latifolia* leaves at a pH of 7.0; **b** LHRH-conjugated AuNPs; **c** LHRH-conjugated AuNPs with PG mixtures; **d** the Scherer ring patterns indicating the fcc gold which is nanocrystalline in nature



octagonal, heptagonal and hexagonal shapes, with varying sizes (Fig. 3a). Similar nanoparticle morphologies were also observed after conjugation and mixture with PG (Fig. 3b and 3c). These combinations of shapes and sizes may be relevant for optimum surface plasmon resonance effect (SPRE) of AuNPs considering the incident angle and AuNPs-laser interaction. The TEM images and selected area electron diffraction (SAED) patterns also confirmed the formation and crystallization of nanoparticles. The SAED pattern presented in Fig. 3d represents the four-fringe pattern of gold nanoparticles, which corresponds to the fcc crystal structure of gold [(111), (200), (220), (311)]. This confirms the formation of pure gold nanoparticles.

The TEM average size distributions of the synthesized AuNPs are shown in Fig. 4a and b, with the average particles size being in the range of 41–50 nm. The hydrodynamic diameter measured with the DLS is presented in Fig. 4c. The DLS measurements of the polydispersity indices of the AuNPs are represented in Fig. 4d. The hydrodynamic diameter of the AuNPs nanoparticles synthesized at a pH of 7.0 was 47.9 nm, while the polydispersity index (PDI) of the same nanoparticles was 0.23. The measured PDIs show that the representative samples of the gold biosynthesized nanoparticles were relatively mono-

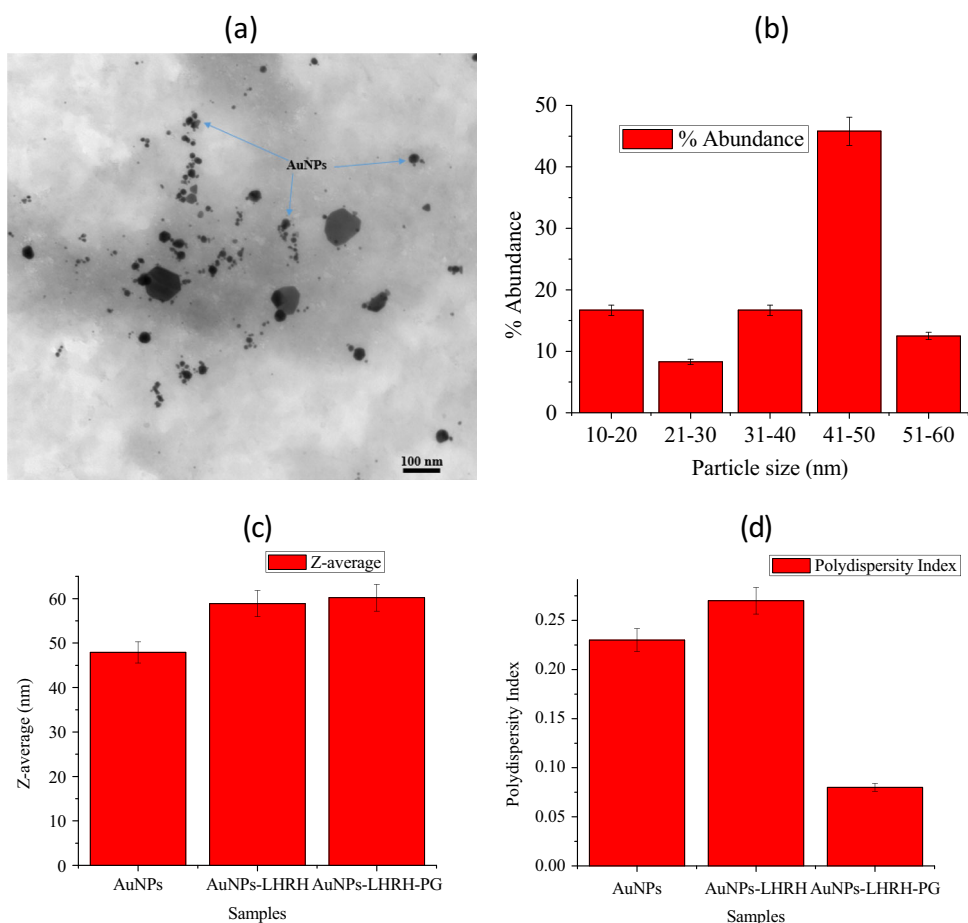
dispersed. The z-averages before conjugation, after conjugation with LHRH, and after the addition of prodigiosin, were 47.9, 58.9 and 60.2 nm, respectively. These are consistent with the findings of Takae et al. [59], who observed an increase in nanoparticle diameter (from 20 to 33.3 nm) after functionalization with 6000 Mw PEG. Some other researchers also have reported DLS measurements of the hydrodynamic diameters of gold nanoparticle to increase from 28.2 to 48.5 nm, with the addition of PEG coatings [60, 61].

Typical EDS results obtained from the AuNPs synthesized at a pH of 7.0 conditions are presented in Fig. 5. The results show clear and predominant evidence of gold peaks, although peaks corresponding to some of the materials (used in the reactions) were also observed (Fig. 5b). Note that the carbon and silicon peaks are attributed to the specimen mount in the SEM grid [62]. The presence of gold peaks is consistent with the existence of gold nanoparticles.

#### 4.2 Adhesion force measurements

The SEM images of the bare AFM tip, AuNPs coated AFM tip, AuNPs-LHRH coated tips and LHRH-conjugated AuNPs/PG mixture are presented in Figs. 6a–6d,

**Fig. 4** **a** and **b** Typical TEM of AuNPs and size distribution; **c** typical DLS hydrodynamic diameter of size distribution of AuNPs synthesized from *Nauclea latifolia* leaves and **d** shows the polydispersity index of AuNPs, AuNPs-LHRH and AuNPs-LHRH-PG, respectively



respectively. When coated with plain gold nanoparticles, the attachment was seen as sparsely scattered on the tip, but the coating with AuNPs-LHRH conjugated gold nanoparticles showed an even attachment as seen from the peeled off region. The SEM images of the coated tips clearly show the presence of AuNPs on the apex of the AFM tips [Fig. 6b–d]. In Fig. 7, a typical AFM–force/distance curve measured by the AFM-cantilever versus tip sample distance was presented. It shows the AFM force-displacement behavior between AuNPs-LHRH coated AFM tips to MDA-MB 231 breast cancer cells AFM-force/distance measurement.

The measured adhesion force between the different constituents and breast cancer cell/normal breast cells are represented in Fig. 8. The resulting pull-off/interaction forces between the bare AFM tip and the breast cancer cells (MDA MB 231 cells) are slightly more than those between bare tips and normal breast cells. In the case of AuNPs coated AFM tips, the interaction between AuNP-coated AFM tips and normal breast cells is less than a factor of two to those with breast cancer cells ( $18.6 \pm 0.93$  nN <  $48.5 \pm 2.5$  nN). In the case of the adhesion forces between LHRH ligand and breast cancer cells or normal breast cells, the pull-off forces obtained were  $21.7 \pm 1.8$  nN and  $105.6 \pm 5.3$

nN, respectively. Furthermore, the adhesion between LHRH-conjugated AuNPs and breast cancer cells or normal breast cells were measured to be  $125.6 \pm 6.3$  nN and  $35.3 \pm 1.8$  nN, respectively. These results clearly show that LHRH-conjugated AuNPs can be used for selective and specific targeting of triple negative breast cancer cells. Finally, the interaction between LHRH-conjugated AuNPs/PG mixtures to breast cancer cells was ( $118.4 \pm 6$  nN) greater than for those with normal breast cells ( $43.4 \pm 2.7$  nN).

## 5 Discussion

Gold nanoparticles exhibit distinct optical and physical properties based on their size (diameter), shape, surface structure and agglomeration state. When functionalizing gold nanoparticles with chemical groups or biomolecules, it is imperative to characterize them. Gold nanoparticles exhibit unique optical feature often known as surface plasmon resonance (SPR), which is, the collective oscillation of electrons in the conduction band of gold nanoparticles in resonance with a specific wavelength of incident light [63]. SPR of gold nanoparticles results in a strong



**Fig. 5** EDX showing elemental composition of **a** AuNPs synthesized from *Nauclea latifolia* at a pH 7.0; **b** LHRH-conjugated AuNPs/PG mixture

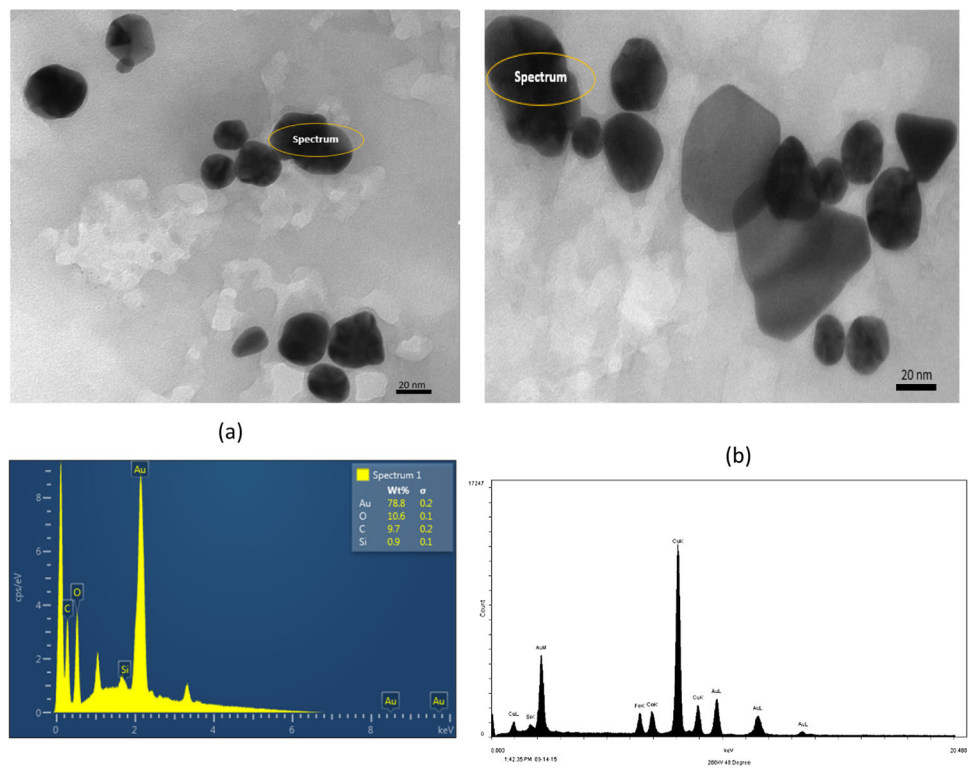
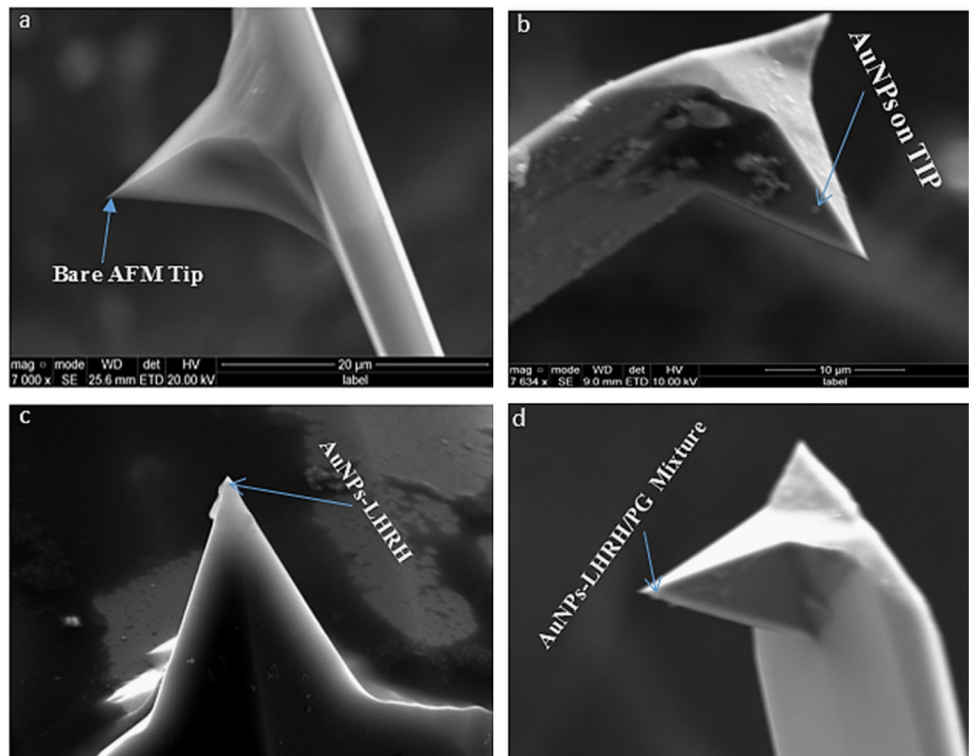


**Fig. 6** Scanning Electron Microscopy image of AFM tips: **a** Bare tip; **b** AuNPs coated AFM tip; **c** LHRH-conjugated AuNPs coated AFM tip; **d** AuNPs-LHRH/PG drug coated AFM tip



absorbance band in the visible region (500–600 nm), which can be measured by UV–Vis spectroscopy. From our results, the SPR of the AuNPs occurred at 540 nm. The SPR

spectrum depends on the size and shape of gold nanoparticles. The production of gold nanoparticles has been correlated with the change in color of pale yellow plant

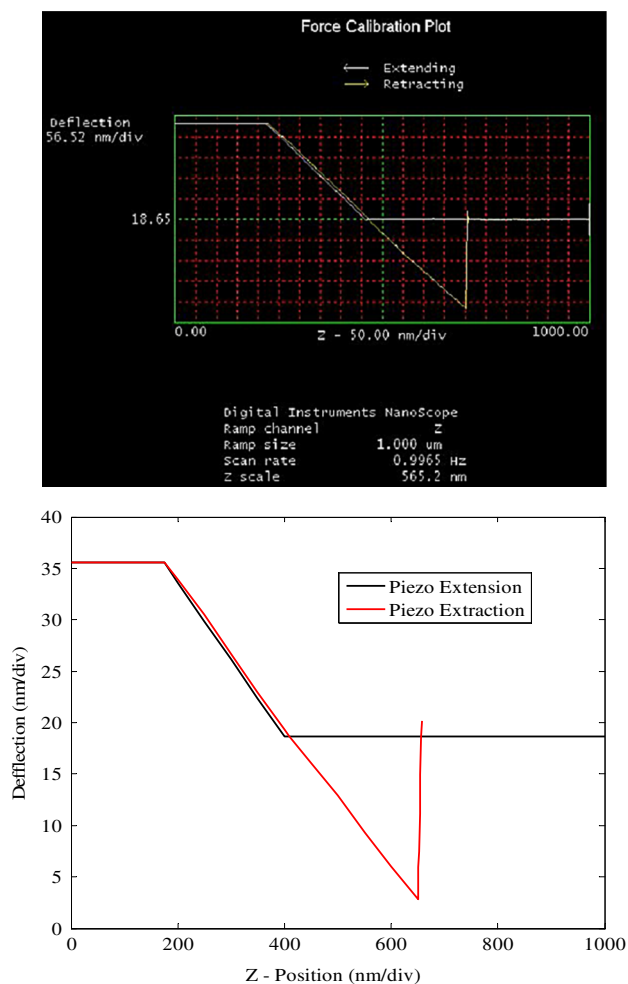


**Fig. 7** Typical AFM force-displacement behavior between AuNPs-LHRH coated AFM tips to MDA-MB 231 breast cancer cells

extracts or bacterial cell suspensions to pink or purple [64, 65]. This color change is as a result of the reduction of  $\text{Au}^{3+}$  to  $\text{Au}^0$  [66]. Detailed results of the synthesis of AuNPs from *Nauclea latifolia* are reported in Ref. [27].

UV-Vis measurements was also be used to evaluate the functionalization of gold nanoparticles. Upon binding of ligands to the gold nanoparticle surface, the SPR spectrum had a red-shift by a few nanometers, as shown in Fig. 2b. This shift has been attributed to the increase in the local refractive index at the gold nanoparticle surface.

The results of the selected area electron diffraction (SAED) patterns indicated the crystallization of nanoparticles. The observed Scherer ring pattern is consistent with the reference face-centered cubic (fcc) gold, indicating that the biogenic nanoparticles seen in the TEM images are indeed crystalline gold. Typical size distributions obtained from the image analyses of the TEM images were compared to those obtained from the DLS measurements in Fig. 4. The measured hydrodynamic diameter describes the dimensions of a sphere that has the same diffusion

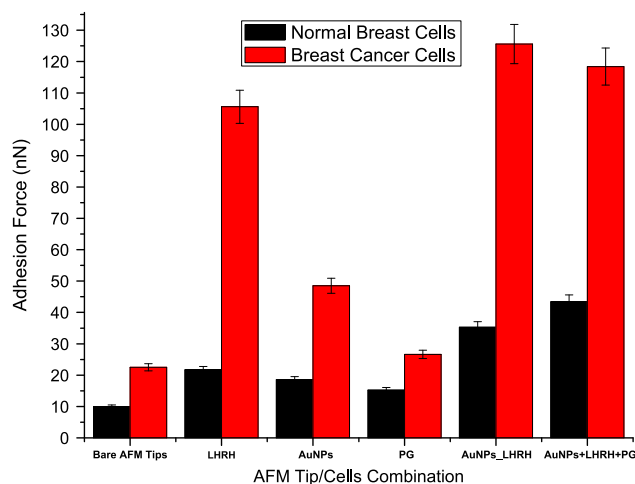
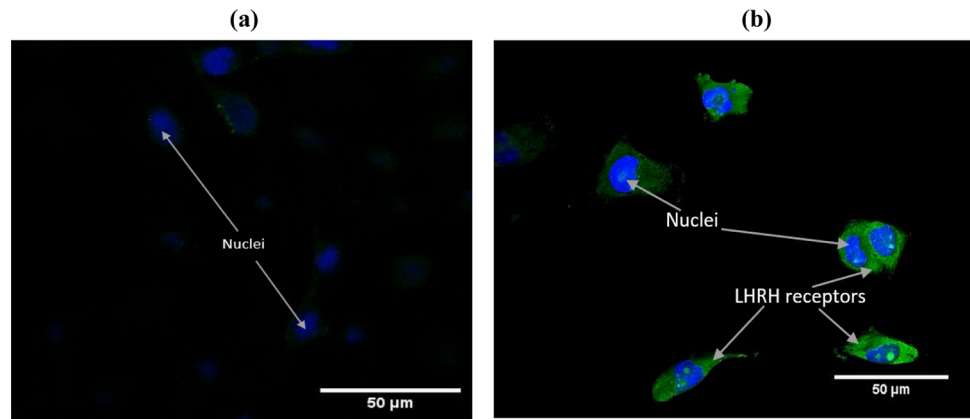


**Fig. 8** Summary of adhesion force measurements between uncoated/bare AFM tip as well as different nanoparticles-coated AFM tips and breast cancer (MDA-MB-231) cells/normal breast (MCF 10 A) cells

coefficients within the same viscous environment. Furthermore, a comparison of the hydrodynamic diameters and the polydispersity index of the gold nanoparticles synthesized (before and after conjugation) was studied. The z-average increased with the addition of the ligand, LHRH, and further when the anti-cancer drug, prodigiosin (PG), was added. This finding was also reported by Takae et al. [59], who observed an increase in nanoparticle diameter (from 20 to 33.3 nm) after functionalization with 6000 Mw PEG. The results obtained from the measurements of the PDI showed a decrease with the addition of the ligands. This suggests that conjugation improves the dispersity of the particles. The AuNPs synthesized at a pH of 7.0 had a PDI of 0.23 before conjugation, PDI of 0.29 after conjugation, and a PDI of 0.08 after conjugation with LHRH and the addition of PG cancer drug.

As discussed earlier, the TEM images correspond to electron transmission through the nanoparticles, while the DLS correspond to the hydrodynamic diameters. The hydrodynamic diameters measured from the DLS were generally much greater than the effective diameters obtained from the TEM images. This is partly due to the adsorption of proteins and organic wastes onto the surfaces of the AuNPs, which is accounted for in the DLS measurements [67]. Such adsorption tends to promote the formation of nanoparticle clusters that increase the hydrodynamic radii. In the case of the TEM measurements, they only account for the electron transmission through the nanoparticle core. Thus, the high magnification TEM images required for the measurement of individual nanoparticle sizes may not necessarily reveal the statistical variations in the cluster sizes that are formed due to nanoparticle aggregation [67]. The EDS analysis revealed the presence of gold (Au), iron

**Fig. 9** Fluorescence confocal images of LHRH receptor distribution on **a** normal breast cells and **b** breast cancer cells. The images show the over-expression of LHRH receptors and nuclei designated by *arrows*



(Fe), which is usually attached to prodigiosin, Cu and Si, which are most likely to be from the sample grid.

The atomic force microscope (AFM) is an imaging device capable of atomic resolution [68]. The AFM employs a small probe on a cantilever, which deflects in response to the intermolecular attractive and repulsive forces found in proximity to the sample [69, 70]. The AFM tips, both coated and uncoated were imaged using the SEM to ensure that the delamination of coating on the AFM tips did not occur during the pull-off/adhesion experiments.

From our results, it is clear that the interaction between LHRH coated AFM tip with breast cancer cells was greater than those of normal cells by a factor of 5. This partly explains why LHRH specifically targets of triple negative breast cancer cells [62, 71–74].

In the case of therapeutics, the PG interaction to breast cancer cells or normal breast cells was measured. This result was important to understand the behavior of PG when used in a nanocluster of AuNPs-LHRH-PG. The adhesion forces between the PG drug and breast cancer cells or normal cells were relatively low, and within the same range.

The higher adhesion values obtained for the LHRH-conjugated AuNPs component to breast cancer cells are attributed to the over-expression of LHRH receptors on cancer cells compared to normal cells (Fig. 9). The increased adhesion between the LHRH-conjugated nanoparticles to breast cancer cells has been shown to be due to the increased incidence of LHRH-receptors on breast cancer cells [61, 62, 71–74]. The results suggest that the over-expressed LHRH receptor, located on breast cancer cells, interact very strongly with LHRH peptides, respectively.

The current results suggest that force microscopy techniques incorporated with LHRH-conjugated AuNPs presented here may be used as a method for the fast screening of ligand-conjugated nanoparticles that can be used for the early detection of other forms of cancer and other diseased cells that over-express ligand receptors on their membrane surfaces. Such over-expression should increase the potential

for the specific targeting and treatment of triple negative breast cancer.

## 6 Summary and concluding remarks

This paper presents the results of a study of adhesion of biosynthesized gold and gold/prodigiosin nanoparticles to triple negative breast cancer cells. We argue that such adhesion could increase the potential for specific targeting and cancer therapy. The AuNPs were synthesized from *Nauclea latifolia* leaf extracts. The adhesion results show that the adhesion force between LHRH-conjugated biosynthesized AuNPs and the breast cancer cell line MDA-MB-231 was greater (by a factor of five) than that of LHRH-conjugated AuNPs to normal breast cells. Similarly, in the case of the nanocluster of AuNPs-LHRH-PG mixture, the adhesion of the mixture to breast cancer cells is greater than that to normal breast cells. The increase in adhesion of the LHRH-conjugated gold nanoparticles is associated with the increased incidence of LHRH receptors that are over-expressed on the surfaces of breast cancer cells. The increased incidence of LHRH receptors in increased adhesive interactions by a factor of about five. It also increases the potential for use of AuNPs-LHRH-PG in the selective and specific targeting and treatment of breast cancer by localized cancer drug delivery, hyperthermia and laser surgery.

**Acknowledgements** The research was supported by the SHESTCO-AUST-Princeton World Bank STEP-B Program, the World Bank African Centers of Excellence Program, Pan African Materials Institute (PAMI) the African Capacity Building Foundation (ACBF), the African Development Bank (ADB) and the Princeton University Old Schools Innovation Fund for their financial support. The authors are also grateful to Ms. Jingjie Hu, Ms. Cathy Chi, Ms. Vanessa Ozonwanne and Mr. Gerald Poirier of Princeton University, for all their assistance in DLS and TEM measurements.

### Compliance with ethical standards

**Conflict of interest** The authors declare that they have no competing interests.

## References

- Jennings T, Strouse G. Past, present and future of gold nanoparticles. *Adv Exp Med Biol.* 2007;620:34–47.
- Holiday R. Use of gold in medicine and surgery. UK: Biomedical Scientist (The Official Gazette of the Institute of Biomedical science; 2008. p. 962–3.
- Dykman LA, Khlebtsov NG. Gold nanoparticles in biology and medicine: recent advances and prospects. *Acta Nat.* 2011;3(2):34–55.
- Chen PO, Mwakwari SC, Oyelere AK. Gold nanoparticles: from nanomedicine to nanosensing. *Nanotechnol, Sci Appl.* 2008;1:45–66.
- Canizal G, Ascencio JA, Gardea-Torresday J, Jose-Yacaman M. Multiple twinned gold nanorods grown by bio-reduction techniques. *J Nanopart Res.* 2001;3:475–81.
- Zhou Y, Yu SH, Cui XP, Wang CY, Chen ZY. Formation of silver nanowires by a novel solid-liquid phase arc discharge method. *Chem Mater.* 1999;11:545–6.
- Sun Y, Mayers B, Herricks T, Xia Y. Polyol synthesis of uniform silver nanowires: a plausible growth mechanism and the supporting evidence. *Nano Lett.* 2003;3:955–60.
- Mouxiang F, Qingbiao L, Daohua S, Yinghua L, Ning H, Xu D, Huixuan W, Jiale H. Rapid preparation process of silver nanoparticles by bioreduction and their characterizations. *chin. J Chem Eng.* 2006;14(1):114–7.
- Selvakannan PR, Mandal S, Pasricha R, Adyanthaya SD, Sastry M. One-step synthesis of hydrophobized gold nanoparticles of controllable size by the reduction of aqueous chloroaurate ions by hexadecylaniline at the liquid-liquid interface. *Chem Commun.* 2002;13:1334–5.
- Okitsu K, Yue A, Tanabe S, Matsumoto H, Yobiko Y. Formation of colloidal gold nanoparticles in an ultrasonic field: control of rate of gold (III) reduction and size of formed gold particles. *Langmuir.* 2001;17(25):7717–20.
- Singh A, Jain D, Upadhyay MK, Khandelwal N, Verma HN. Green synthesis of silver nanoparticles using *Argemone mexicana* leaf extract and evaluation of their antimicrobial activities. *Dig J Nanomater Biostruct.* 2010;5(2):483–9.
- Leela A, Vivekanandan M. Tapping the unexploited plant resources for the synthesis of silver nanoparticles. *Afr J Biotechnol.* 2008;7(17):3162–5.
- Balaprasad A. Biosynthesis of Gold Nanoparticles (Green-Gold) Using Leaf Extract of Terminalia Catappa. *E-J Chem.* 2010;7(4):1334–9.
- Gericke M, Pinches A. Microbial production of gold nanoparticles. *Gold Bull.* 2006;39(1):22–8.
- Sanghi R, Verma P, Puri S. Enzymatic formation of gold nanoparticles using *Phanerochaete Chrysosporium*. *Adv Chem Eng Sci.* 2011;1(3):154–62.
- Sun Y, Xia Y. Shape-controlled synthesis of gold and silver nanoparticles. *Science.* 2002;298(5601):2176–9.
- Nair B, Pradeep T. Coalescence of nanoclusters and formation of submicron crystallites assisted by Lactobacillus Strains. *Cryst Growth Des.* 2002;2:293.
- Chatterjee DK, Diagarjane P, Krishnan S. Nanoparticle-mediated hyperthermia in cancer therapy. *Ther Deliv.* 2011;2(8):1001–14.
- Mafune F, Kohno J, Takeda Y. Full physical preparation of size-selected gold nanoparticles in solution: laser ablation and laser-induced size control. *J Phys Chem B.* 2002;106(31):7575–7.
- Cho K, Wang X, Nie S, Chen ZG, Dong MS. Therapeutic nanoparticles for drug delivery in cancer. *Clin Cancer Res.* 2008;14(5):1310–6.
- Mukherjee P, Ahmad A, Mandal D, Senapati S, Sainkar SR, Khan MI, Parischa R, Ajayakumar PV, Alam M, Kumar R, Sastry M. Fungus mediated synthesis of silver nanoparticles and their immobilization in the mycelial matrix: A novel biological approach to nanoparticle synthesis. *Nano Lett.* 2001;1:515–9.
- Ahmad A, Senapati S, Khan MI, Kumar, Sastry M. Extracellular biosynthesis of monodisperse fold nanoparticles by a novel extremophilic actinomycete *thermonospora* sp. *Langmuir.* 2003;19:3550–3.
- Stephen JR, Maenaughton SJ. Developments in terrestrial bacterial remediation of metals. *Curr Opin Biotechnol.* 1999;10:230–5.
- Sastry M, Ahmad A, Khan MI, Kumar R. Biosynthesis of metal nanoparticles using fungi and actinomycete. *Curr Sci.* 2003;85:162–70.
- Huang J, Li Q, Sun D, Lu Y, Su Y, Yang X, Wang H, Wang Y, Shao W, He N, Hong J, Chen C. Biosynthesis of silver and gold nanoparticles by novel sundried *Cinnamomum camphora* leaf. *Nanotechnology.* 2007;18(10):105104–15.
- Kasthuri J, Kathiravan K, Rajendiran N. Phyllanthin-assisted biosynthesis of silver and gold nanoparticles: a novel biological approach. *J Nanopart Res.* 2009;11(5):1075–85.
- Dozie-Nwachukwu SO, Etuk-Udo G, Obayemi JD, Anuku N, Odusanya OS, Malatesta K, Chi C, Soboyejo WO. Biosynthesis of gold nanoparticles from *Nauclea latifolia* leaves. *Adv Mater Res.* 2016;1132:36–50.
- Pellegrino T, Kudera S, Liedl T, Muñoz Javier A, Manna L, Parak WJ. On the development of colloidal nanoparticles towards multifunctional structures and their possible use for biological applications. *Small.* 2005;1:48–63.
- Shankar SS, Ahmad A, Pasricha R, Sastry M. Bioreduction of chloroaurate ions by geranium leaves and its endophytic fungus yields gold nanoparticles of different shapes. *J Mater Chem.* 2003;13:1822–6.
- Ankamwar B, Chaudhary M, Sastry M. Gold nanotriangles biologically synthesized using tamarind leaf extract and potential application in vapor sensing. *Synth React Inorg Metal-Org Nano-Metal Chem.* 2005;35:19–26.
- Huang J, Li Q, Sun D, Lu Y, Su Y, Yang X. Biosynthesis of silver and gold nanoparticles by novel sundried *Cinnamomum camphora* leaf. *Nanotechnology.* 2007;18:105104–14.
- Shankar SS, Rai A, Ahmad A, Sastry M. Controlling the optical properties of lemongrass extract synthesized gold nanotriangles and potential application in infrared-absorbing optical coatings. *Chem Mater.* 2005;17:566–72.
- Ankamwar B, Damle C, Ahmad A, Sastry M. Biosynthesis of gold and silver nanoparticles using *Embllica officinalis* fruit extract, their phase transfer and transmetallation in an organic solution. *J Nanosci Nanotechnol.* 2005;5:1665–71.
- Shankar SS, Rai A, Ahmad A, Sastry M. Rapid synthesis of Au, Ag and bimetallic Au core–Ag shell nanoparticles using neem (*Azadirachta indica*) leaf broth. *J Colloid Interf Sci.* 2004;275:496–502.
- Chandran SP, Chaudhary M, Pasricha R, Ahmad A, Sastry M. Synthesis of gold nanotriangles and silver nanoparticles using *Aloe vera* plant extract. *Biotechnol Prog.* 2006;22:577–83.
- Umadevi M, Sampath Kumar KP, Bhowmik D, Duraive S. Traditionally used anticancer herbs in India. *J Med Plants Stud.* 2013;1(3):56–74.
- Paul J, Gnanam RM, Jayadeepa R, Arul L. Anti-cancer activity on Graviola, an exciting medicinal plant extract vs various cancer cell lines and a detailed computational study on its potent anti-cancerous leads. *Curr Top Med Chem.* 2013;13(14):1666–73.
- Akpanabiatu MI, Umoh IB, Eyong EU, Udoh FV. Influence of *Nauclea latifolia* leaf extracts on some hepatic enzymes of rats fed on coconut oil and non-coconut oil meals. *Pharm Biol.* 2005;43(2):153–7.

39. Brandenburg KS, Shakeri-Zadeh A, Mansoori GA. Folate-conjugated gold nanoparticles for cancer nanotechnology applications. *Nanotechnology*. 2011;3:404–7.
40. Gao T, Hong H, Sun J. Applications of gold nanoparticles in cancer nanotechnology. *Nanotechnol, Sci Appl*. 2008;1:17–32.
41. Chatterjee DK, Diagaradjane P, Krishnan S. Nanoparticle-mediated hyperthermia in cancer therapy. *Ther Deliv*. 2011;2(8):1001–14.
42. Jain S, Hirst DG, O'Sullivan JM. Gold nanoparticles as novel agents for cancer therapy. *Br J Radiol*. 2012;85(1010):101–13.
43. Hampf E, Botah R, Odusanya SO, Anuku N, Malatesta K, Soboyejo WO. Biosynthesis and adhesion of gold nanoparticles for breast cancer detection and treatment. *J Mater Res*. 2012;27(22):2891.
44. Meng J, Paetzell E, Bogorad A, Soboyejo WO. Adhesion between peptides/antibodies and breast cancer cells. *J Appl Phys*. 2010;107:114301.
45. Oni Y, Hao K, Dozie-Nwachukwu S, Obayemi JD, Odusanya OS, Anuku N, Soboyejo WO. Gold nanoparticles for cancer detection and treatment: the role of adhesion. *J Appl Phys*. 2014;115:084305.
46. Gates RS, Osborn WA, Pratt JR. Experimental determination of mode correction factors for thermal method spring constant calibration of AFM cantilevers using laser Doppler vibrometry. *Nanotechnology*. 2013;24(25):255706.
47. Dupres V, Menozzi FD, Loch C, Clare BH, Abbott NL, Cuenot S, Bompard C, Raze D, Dufrene YF. Nanoscale mapping and functional analysis of individual adhesins on living bacteria. *Nat Methods*. 2005;2:515–20.
48. Wojcikiewicz EP, Zhang X, Moy V. Force and compliance measurements on living cells using atomic force microscopy (AFM). *Biol Proced*. 2004;6:1–9.
49. Li F, Redick SD, Erickson HP, Moy VT. Force measurements of the  $\alpha 5\beta 1$  Integrin–Fibronectin interaction. *Biophys J*. 2003;84:1252–62.
50. Shiao-Wen T, Jiunn-Woei TL, Fu-Yin H, Yi-Yun C, Mei-Jhih L, Ming-His Y. Surface-modified gold nanoparticles with folic acid as optical probes for cellular imaging. *Sensors*. 2008;8:6660–73.
51. Obayemi JD, Danyuo Y, Dozie-Nwachukwu S, Odusanya OS, Anuku N, Malatesta K, Yu W, Uhrich KE, Soboyejo O. PLGA-based microparticles loaded with bacterial-synthesized prodigiosin for anticancer drug release: Effects of particle size on drug release kinetics and cell viability. *Mater Sci Eng C*. 2016;66:51–65.
52. Kamble KD, Hiwarale VD. "Prodigiosin production from *Serratia marcescens* strains obtained from farm soil". *Int J Environ Sci*. 2012;3(1):631–8.
53. Butt H, Cappella B, Kappl M. Force measurements with the atomic force microscope: technique, interpretation and applications. *Surf Sci Rep*. 2005;59:1–152.
54. Santner E, Stegemann B. Adhesion measurements by AFM – a gateway to the basics of friction. Accessed from: [www.academia.edu/7351106/Adhesion\\_measurements\\_by\\_AFM\\_a\\_gateway\\_to\\_the\\_basics\\_of\\_friction](http://www.academia.edu/7351106/Adhesion_measurements_by_AFM_a_gateway_to_the_basics_of_friction) on 30th March, 2016.
55. Bhushan B, (Ed.). *Handbook of Micro/Nanotribology*. 2nd ed. Boca Raton: CRC press; 1999.
56. Burnham NA, Colton RJ, Pollock HM. Interpretation of force curves in force microscopy. *Nanotechnology*. 1993;4:64–80.
57. Cappella B, Dietler G. Force-distance curves by atomic force microscopy. *Surf Sci Rep*. 1999;34(1-3):1–104.
58. Rogošić M, Mencer HJ, Gomzi Z. Polydispersity index and molecular weight distributions of polymers. *Eur Polym J*. 1996;32(11):1337–44.
59. Takae S, Akiyama Y, Otsuka H, Nakamura T, Nagasaki Y, Kataoka K. Ligand density effect on biorecognition by PEGylated gold nanoparticles: regulated interaction of RCA120 lectin with lactose installed to the distal end of tethered PEG N strands on gold surface. *Biomacromolecules*. 2005;6(2):818–24.
60. Hall JB, Dobrovolskaia MA, Patri AK, McNeil SE. Characterization of nanoparticles for therapeutics. *Nanomedicine*. 2007;2(6):789–803.
61. Arnida A, Janát-Amsbury MM, Ray A, Peterson CM, Ghandehari H. Geometry and surface characteristics of gold nanoparticles influence their biodistribution and uptake by macrophages. *Eur J Pharm Biopharm*. 2011;77:417–23.
62. Obayemi JD, Dozie-Nwachukwu S, Danyuo Y, Odusanya OS, Anuku N, Malatesta K, Soboyejo WO. Biosynthesis and the conjugation of magnetite nanoparticles with Luteinizing hormone releasing hormone (LHRH). *J Mater Sci Eng C*. 2015;46:482–96.
63. Xiaohua Huang, Mostafa A. El-Sayed. Gold nanoparticles: Optical properties and implementations in cancer diagnosis and photothermal therapy. *J Adv Res*. 2010;1(1):13–28.
64. Boham AB, Kocipai AA.: Flavonoids and condensed tannins from leaves of Hawaiian *Vaccinium vaticulation* and *V. calycinium*. *Pac Sci*. 1994;48:458–63.
65. Madhavi RB, Dighe VV. Synthesis of gold nano particles using *Putranjiva roxburghii* wall. Leaves extract. *Int J Drug Discov Herbal Res*. 2012;2(1):275–8.
66. Kundu A, Layek RK, Kujla Nandi AK. : Highly fluorescent graphene oxide-poly (vinyl alcohol) hybrid: an effective material for specific Au<sup>3+</sup> ion sensors. *ACS Appl Mater Interface*. 2012;4(10):5576–82.
67. Lim J, Yeap SP, Che HX, Low SC. Characterization of magnetic nanoparticle by dynamic light scattering. *Nanoscale Res Lett*. 2013;8:381.
68. Ohnesorge F, Binnig G. True atomic resolution by atomic force microscopy through repulsive and attractive forces. *Science*. 1993;260(5113):1451–6.
69. Binnig G, Quate CF, Gerber C. Atomic force microscope. *Phys Rev Lett*. 1986;56(9):930–3.
70. Martin Y, Williams CC, Wickramasinghe HK. Atomic force microscope-force mapping and profiling on a sub 100-Å scale. *J Appl Phys*. 1987;61(10):4723–9.
71. Zhou J, Leuschner C, Kumar C, Hormes JF, Soboyejo WO. Sub-cellular accumulation of magnetic nanoparticles in breast tumors and metastases. *Biomaterials*. 2006;27(9):2001–8.
72. Zhou J, Leuschner C, Kumar C, Hormes J, Soboyejo WOA. TEM study of functionalized nanoparticles targeting breast cancer cells in mice. *Mater Sci Eng C*. 2006;26:1451–5.
73. Leuschner C, Kumar CSSR, Hansel W, Zhou J, Soboyejo WO, Hormes J. LHRH-Conjugated magnetic iron oxide nanoparticles for detection of breast cancer metastases. *Breast Cancer Res Treat*. 2006;99:163–76.
74. Meng J, Fana J, Galiana G, Branca RT, Clasen PL, Ma, S, Zhou J, Leuschner C, Kumar CSSR., Hormes J, Otit, T, Beye AC, Harmer MP, Kiely CJ, Warren W, Haataja MP, Soboyejo WO. LHRH-functionalized superparamagnetic iron oxide nanoparticles for breast cancer targeting and contrast enhancement in MRI. *Mater Sci Eng C*. 2009; 29: 1467-79.